ATGL and DGAT1 are involved in the turnover of newly synthesized triacylglycerols in hepatic stellate cells[S]

Maidina Tuohetahuntila,* Martijn R. Molenaar,* Bart Spee,† Jos F. Brouwers,* Martin Houweling,* Arie B. Vaandrager,* and J. Bernd Helms[1],*

Departments of Biochemistry and Cell Biology* and Clinical Sciences of Companion Animals,† Faculty of Veterinary Medicine and Institute of Biomembranes, Utrecht University, 3584 CM Utrecht, The Netherlands

Abstract **Hepatic stellate cell (HSC) activation is a critical step in the development of chronic liver disease. During activation, HSCs lose their lipid droplets (LDs) containing triacylglycerol (TAG), cholesteryl esters (CEs), and retinyl esters (REs). Here we aimed to investigate which enzymes are involved in LD turnover in HSCs during activation in vitro. Targeted deletion of the *Atgl* gene in mice HSCs had little effect on the decrease of the overall TAG, CE, and RE levels during activation. However, ATGL-deficient HSCs specifically accumulated TAG species enriched in PUFAs and degraded new TAG species more slowly. TAG synthesis and levels of PUFA-TAGs were lowered by the diacylglycerol acyltransferase (DGAT)1 inhibitor, T863. The lipase inhibitor, Atglistatin, increased the levels of TAG in both WT and ATGL-deficient mouse HSCs. Both Atglistatin and T863 inhibited the induction of activation marker, α-smooth muscle actin, in rat HSCs, but not in mouse HSCs. Compared with mouse HSCs, rat HSCs have a higher turnover of new TAGs, and Atglistatin and the DGAT1 inhibitor, T863, were more effective. Our data suggest that ATGL preferentially degrades newly synthesized TAGs, synthesized by DGAT1, and is less involved in the breakdown of preexisting TAGs and REs in HSCs. Furthermore a large change in TAG levels has modest effect on rat HSC activation.**—Tuohetahuntila, M., M. R. Molenaar, B. Spee, J. F. Brouwers, M. Houweling, A. B. Vaandrager, and J. B. Helms. **ATGL and DGAT1 are involved in the turnover of newly synthesized triacylglycerols in hepatic stellate cells.** ***J. Lipid Res.*** **2016.** 57: **1162–1174.**

Supplementary key words vitamin A • lipase • lipolysis and fatty acid metabolism • lipid droplets • lipidomics • heavy isotope labeling • triacylglycerol pools • retinyl esters • adipose triglyceride lipase • diacylglycerol acyltransferase 1

Hepatic stellate cells (HSCs) are the main vitamin A (retinol)-storing cells of the body (1, 2). In a healthy liver, HSCs store vitamin A in the form of retinyl esters (REs) in large lipid droplets (LDs), together with triacylglycerols (TAGs) and cholesteryl esters (CEs). HSCs are located in the space of Disse, between the sinusoidal endothelial cells and the hepatocytes. Upon liver injury, quiescent HSCs can transdifferentiate into an activated myofibroblastic phenotype (1). Activated macrophages, in concert with the HSCs, may initiate this transition by secreting cytokines, such as transforming growth factor β (TGF-β), which stimulate the synthesis of matrix proteins and the release of retinoids by HSCs (1, 3). The loss of retinoids is associated with a gradual disappearance of the LDs inside the HSCs. We previously reported that LD degradation in activated rat HSCs occurs in two phases (4). Upon activation of the HSCs, the LDs reduce in size, but increase in number, during the first 7 days in culture before they disappear in a later phase. Raman and lipidomic studies showed that in the initial phase of HSC activation, the REs disappear rapidly, whereas the TAG content is transiently increased (4). Interestingly, this increase in TAGs in rat HSCs is predominantly caused by a large and specific increase in PUFA-containing TAG species during the first 7 days in culture, mediated by an increase in expression of the PUFA-specific FA, long-chain acyl-CoA synthase (ACSL)4, and a decrease in expression of the other ASCLs, especially ASCL1 (5). So far, the molecular mechanisms and identity of the enzymes involved in the observed increase in LD number and their subsequent breakdown during HSC activation are not well understood. An increase in number can be accomplished by the de novo synthesis of new LDs (6) or fission of existing large LDs (7). Breakdown of LDs is best characterized in adipose cells, in which key roles are assigned to adipose triglyceride lipase [ATGL, also known as patatin-like phospholipase domain containing (PNPLA)2], its coactivator, CGI-58, and hormone-sensitive lipase (HSL) (8). The first two proteins are known

This work was supported by the Seventh Framework Programme of the European Union-funded "LipidomicNet" project (proposal number 202272).

Manuscript received 8 January 2016 and in revised form 26 April 2016.

Published, JLR Papers in Press, May 14, 2016
DOI 10.1194/jlr.M066415

Abbreviations: ACSL, long-chain acyl-CoA synthetase; APCI, atmospheric pressure chemical ionization; ATGL, adipose triglyceride lipase; CE, cholesteryl ester; DAG, diacylglycerol; DGAT, diacylglycerol acyltransferase; HSC, hepatic stellate cell; HSL, hormone-sensitive lipase; LAL/Lipa, lysosomal acidic lipase; LD, lipid droplet; PF, paraformaldehyde; PNPLA, patatin-like phospholipase domain containing; RE_1 retinyl ester; α-SMA, α-smooth muscle actin; TAG, triacylglycerol.

[1] To whom correspondence should be addressed.
e-mail: J.B.Helms@uu.nl

[S] The online version of this article (available at http://www.jlr.org) contains a supplement.

to have a more general function, as deficiencies in either one lead to neutral lipid storage diseases (9). Both ATGL and CGI-58 were present on LDs in the HSC line, HSC-T6 (10), and rat HSCs were shown to express ATGL, although it was downregulated upon activation (11). In mouse HSCs, lipid breakdown was shown to be partially mediated by a lipophagic pathway, as inhibition of autophagy increased the amount of LDs (12, 13). Because inhibition of autophagy was shown to impair HSC activation in mice and this effect could be partially reversed by addition of exogenous FAs, it was suggested that LD breakdown is required to fulfill the energy demands of HSCs during activation (13). On the other hand, HSC activation was shown to be relatively undisturbed in the absence of REs and LDs in lecithin:retinol acyltransferase (LRAT) knockout mice (14).

In this study, we addressed the question of whether a change in lipid metabolism is causally related to the activation process in rat and mouse HSCs. We identified enzymes involved in LD formation and breakdown in HSCs in vitro and studied the effect of inhibition of these enzymes on HSC activation.

MATERIALS AND METHODS

Reagents

D4-palmitate, D8-arachidonate, and Atglistatin were purchased from Cayman Chemical (Ann Arbor, MI). DMEM, FBS, and penicillin/streptomycin were obtained from Gibco (Paisley, UK). BSA fraction V was obtained from PAA (Pasching, Austria). T863 and collagenase (*Clostridium histolyticum* type I) was obtained from Sigma-Aldrich (St. Louis, MO), and saponin from Riedel-de Haën (Seelze, Germany). The mouse monoclonal antibody against α-smooth muscle actin (α-SMA) was from Thermo Scientific (Waltham, MA). LD staining dye, LD540, was kindly donated by Dr. C. Thiele, Bonn, Germany. Hoechst 33342 was obtained from Molecular Probes (Paisley, UK), paraformaldehyde (PF) (8%) was obtained from Electron Microscopy Sciences (Hatfield, PA). FluorSave was obtained from Calbiochem (Billerica, MA), all HPLC-MS solvents were from Biosolve (Valkenswaard, The Netherlands) with the exception of chloroform (Carl Roth, Karlsruhe, Germany) and were of HPLC grade. Silica-G (0.063–0.200 mm) was purchased from Merck (Darmstadt, Germany).

Animals

We used 10- to 12-week-old male and female $Atgl^{+/+}$ (WT) and $Atgl^{-/-}$ mice, generated by crosses of $Atgl^{+/-}$ C57BL/6J mice (15) and paired on sex and age from the same nest and adult male Wistar rats (300–400 g).

Procedures of mouse and rat care and handling were in accordance with governmental and international guidelines on animal experimentation, and were approved by the Animal Experimentation Committee (Dierexperimentencommissie) of Utrecht University (Dierexperimentencommissie numbers: 2010.III.09.110, 2012.III.10.100, and 2013.III.09.065).

HSC isolation and in vitro primary cell culture

Stellate cells were isolated from livers of mice and rats by collagenase digestion followed by differential centrifugation (16) and cultured, as described previously (5), in DMEM supplemented with 10% FBS, 100 units/ml penicillin, 100 μg/ml streptomycin, and 4 μl/ml Fungizone and cells were maintained in a humidified 5% CO_2 incubator at 37°C. Medium was changed every 3 days.

Gene silencing

Gene-silencing experiments were performed using siRNA for target genes or nontargeting siRNA as a control (ON-TARGETplus SMARTpool of four siRNAs; Thermo-Scientific, Rochester, NY) according to the manufacturer's instructions. Briefly, 2 days after plating, the cells were treated with 40 nM siRNA using 5 μl/ml RNAiMAX (Invitrogen, Breda, The Netherlands) in antibiotic-free complete medium (with FBS). After 6 h of transfection, medium was changed to standard culturing conditions up to day 7.

RNA isolation, cDNA synthesis, and quantitative PCR

Total RNA was isolated from HSCs grown in a 24-well plate using RNeasy Mini kit (Qiagen, Venlo, The Netherlands) including the optional on-column DNase digestion (Qiagen RNase-free DNase kit). RNA was dissolved in 30 μl of RNase-free water and was quantified spectrophotometrically using a Nanodrop ND-1000 (Isogen Life Science, IJsselstein, The Netherlands). An iScript cDNA synthesis kit (Bio-Rad, Veenendaal, The Netherlands) was used to synthesize cDNA. Primer design and quantitative (q) PCR conditions were as described previously (17). Briefly, qPCR reactions were performed in duplicate using the Bio-Rad detection system. Amplifications were carried out in a volume of 25 μl containing 12.5 μl of 2× SYBR Green Supermix (Bio-Rad), 1 ul of forward and reverse primer, and 1 μl cDNA. Cycling conditions were as follows: initial denaturation at 95°C for 3 min, followed by 45 cycles of denaturation (95°C for 10 s), annealing temperature (see supplementary Tables 1, 2) for 30 s, and elongation (72°C for 30 s). To determine the relative expression of a gene, a 4-fold dilution series from a pool of all samples of all genes tested was used. The amplification efficiency was between 95 and 105%, amplicon sequencing confirmed the specificity and for each sample a melt-curve analysis was performed. IQ5 real-time PCR detection system software (Bio-Rad) was used for data analysis. Expression levels were normalized by using the average relative amount of the reference genes. Reference genes used for normalization are based on their stable expression in stellate cells, namely, tyrosine 3-monooxygenase/tryptophan 5-monooxygenase activation protein zeta (*Ywhaz*), hypoxanthine phosphoribosyl transferase (*Hprt*), and hydroxylmethylbilane synthase (*Hmbs*). Primers of reference and target genes are listed in supplementary Tables 1, 2.

Immunofluorescence

Freshly isolated HSCs were grown on glass coverslips in 24-well plates at 37°C for 7 days. Staining of cells was performed as follows: cells were fixed in 4% (v/v) PF at room temperature for 30 min and stored in 1% (v/v) PF at 4°C for a maximum of 1 week. HSCs were washed twice in PBS, permeabilized [0.1% (w/v) saponin] and blocked with 2% BSA for 1 h at room temperature. After blocking, slides were incubated 1 h with the primary antibody against α-SMA (50–75 ug/ml), washed again, and incubated for 1 h with anti-mouse antibody (15 ug/ml) supplemented with Hoechst (4 ug/ml) for nuclear counterstaining and LD dye, LD540 (0.05 ug/ml). Thereafter, coverslips were mounted with FluorSave on microscopic slides. Image acquisition was performed on a Leica TCS SPE-II confocal microscope at the Center of Cellular Imaging, Faculty of Veterinary Medicine, Utrecht University.

To quantify LD size and numbers per cell, confocal images of LD540 (LDs) and Hoechst33342 (nuclei) were analyzed with

CellProfiler v2.1.1. Recognized LDs and nuclei were overlayed on the original image to confirm the identity. The error rate was <5% for LDs and <2% for nuclei.

Determination of TAG turnover

To investigate the dynamics of TAG formation and degradation, we labeled isolated rat HSCs for 1 or 2 days with 25 μM D4-palmitate and 25 μM D8-arachidonate in medium containing 10% fetal calf serum. The labeling medium contained approximately 25% of unlabeled palmitate and 5% of unlabeled arachidonate from the FBS [5–10 μM and 1–2 μM, respectively (18)]. After the labeling, the cells were either harvested or subsequently chased for 1 or 2 days in medium containing 10% fetal calf serum in the absence of the stable isotope-labeled FAs to determine the breakdown of the labeled TAGs.

Analysis of neutral lipids by HPLC-MS

Lipids were extracted from a total cell homogenate of HSCs grown in a 12-well plate by the method of Bligh and Dyer (19) after addition of 200 pmol tripentadecanoylglycerol as internal standard. Lipid extracts were dissolved in methanol/chloroform (1/9, v/v), loaded on top of the silica-G column (approximately 10 mg of 0.063–0.2 mm silica) and separated in a neutral and phospholipid fraction (20). Neutral lipids were eluted with two volumes acetone, dried under nitrogen gas, and stored at −20°C. Prior to HPLC-MS analysis, the neutral lipid fraction was dissolved in methanol/chloroform (1/1, v/v) and separated on a Kinetex /HALO C8-e column (2.6 micron, 150 × 3.00 mm; Phenomenex, The Netherlands). A gradient was generated from methanol/water (5/5, v/v) to methanol/isopropanol (8/2, v/v) at a constant flow rate of 0.3 ml/min. MS of neutral lipids (TAGs, CEs, REs, and cholesterol) was performed using atmospheric pressure chemical ionization (APCI) interface (AB Sciex Instruments, Toronto, ON, Canada) on a Biosystems API-2000 Q-trap. The system was controlled by Analyst version 1.4.2 software (MDS Sciex, Concord, ON, Canada) and operated in positive ion mode using settings described previously (4, 5). Typical TAG, CE, and RE ions detected are shown in supplementary Fig. 1. Cholesterol and CEs give typical ions with a *m/z* of 369, and REs with a *m/z* of 269, due to the loss of the FA chain. It is important to note that TAG species have retention times on HPLC that are characteristic for TAGs. Subsequently, ionization of the TAG species by APCI generates some diacylglycerol (DAG) fragments. As these DAG fragments are generated after HPLC, they have HPLC retention times that are the same as the TAG species that they are derived from. In contrast, DAG species present in HSCs have DAG-specific retention times. TAG fragments with two non-, single-, and double-labeled palmitoyl chains (16:0, 16:0, x) were quantitated by counting ions with *m/z* of 551, 555, and 559, respectively. TAG fragments with a non- or single-labeled palmitoyl chain and an oleoyl chain (16:0, 18:1, x) were quantitated by counting ions with *m/z* of 577 and 581, respectively, and non-, single-, double-, and triple-labeled di-arachidonoyl-palmitoyl-glycerol (20:4, 20:4, 16:0) was quantitated by counting ions with *m/z* of 903, 907+911, 915+919, and 923, respectively. Typical non-labeled, high abundant TAG species quantitated were: non-PUFA 52:3 (*m/z* 859) and 54:3 (*m/z* 885); PUFA 56:5 (*m/z* 909), 58:6 (*m/z* 935), 60:9 (*m/z* 957), and 62:11 (*m/z* 981). Total TAG was determined by quantitating all ions between *m/z* 530 and 1,050 with a retention time of TAG species and corrected for the presence of second and third isotope peaks. In this mass and retention time range, no CEs and REs were detected (see supplementary Fig. 1). The quantitated lipids were normalized to the amount of cholesterol in the same sample. Cholesterol was found to be a good marker for recovery of cellular material, as the cholesterol/protein ratio was found to be constant during HSC culture.

Statistical analysis

Each experiment was performed in duplicate and repeated at least three times. Comparisons of variables between multiple factors were made by a two-way ANOVA. Comparisons of a variable between two groups were made with unpaired or paired Student's *t*-test depending on whether the data were normalized to a control before analysis. Differences were considered statistically significant if the *P* value was less than 0.05.

RESULTS

Differential effect of ATGL on TAG breakdown in mouse HSCs

We investigated the dynamics of neutral lipid breakdown in HSCs isolated from WT and *Atgl*$^{-/-}$ mice. HSCs from *Atgl*$^{-/-}$ mice have almost 2-fold higher TAG levels compared with WT mice during the cell culture period, but similar levels of CEs and REs (**Fig. 1A–C**). These results clearly implicate ATGL in TAG metabolism of HSCs. Surprisingly, however, upon culturing and, hence, activation of HSCs, the TAG levels in ATGL-deficient HSCs dropped with an apparently similar rate as compared with WT (Fig. 1A), indicating that ATGL is not the main lipase in mouse HSCs involved in TAG hydrolysis during activation. Likewise, there was no effect of ATGL knockout on the decrease of CE and RE levels upon culturing (Fig. 1B, C). To look more closely at a possible role of ATGL in lipid breakdown during mouse HSC activation, we quantitated different TAG species individually and expressed the TAG levels as percent of the levels at day 1 (Fig. 1D–F). In particular, TAG species with one or more PUFA moieties were increased in ATGL-deficient HSCs at day 7 and day 14, but decreased in WT HSCs. Non-PUFA-TAG species decreased at an almost similar rate in *Atgl*$^{-/-}$ HSCs. An exact determination of the contribution of the PUFA-TAG species to the total amount of TAG by the APCI-MS method is hampered by the numerous species (>1,000) and the observation that the various TAG species fragment to a different degree depending on the saturation of their acyl chains (5). Nevertheless, quantitation of a number of representative intact and fragmented TAG ions allowed us to estimate that WT HSCs at day 1 have 10% TAGs with one or more PUFAs, whereas this was approximately 5% in *Atgl*$^{-/-}$ HSCs. At day 14, the fraction of PUFA-TAGs in WT HSCs was similar as on day 1, but in ATGL$^{-/-}$ cells it was increased to more than 30% (supplementary Figs. 1D, 2).

This allowed us to estimate that the PUFA-TAG levels in *Atgl*$^{-/-}$ HSCs at days 1, 7, and 14 are 0.13, 0.33, and 0.29 nmol/mmol cholesterol, respectively.

We previously reported that the increase in PUFA-TAGs in WT HSCs upon culturing in vitro was dependent on a preferential incorporation of exogenous FAs into TAG (4, 5). We therefore determined the incorporation and subsequent chase of deuterium-labeled FAs (D4-palmitate and D8-arachidonate) in mouse HSCs. As shown in **Fig. 2A**, approximately 5% of all the TAG species were labeled with D4-palmitate in either TAG (16:0, 16:0, x) or TAG (16:0, 18:1, x) (sum of labeled species in first and fifth bar). The

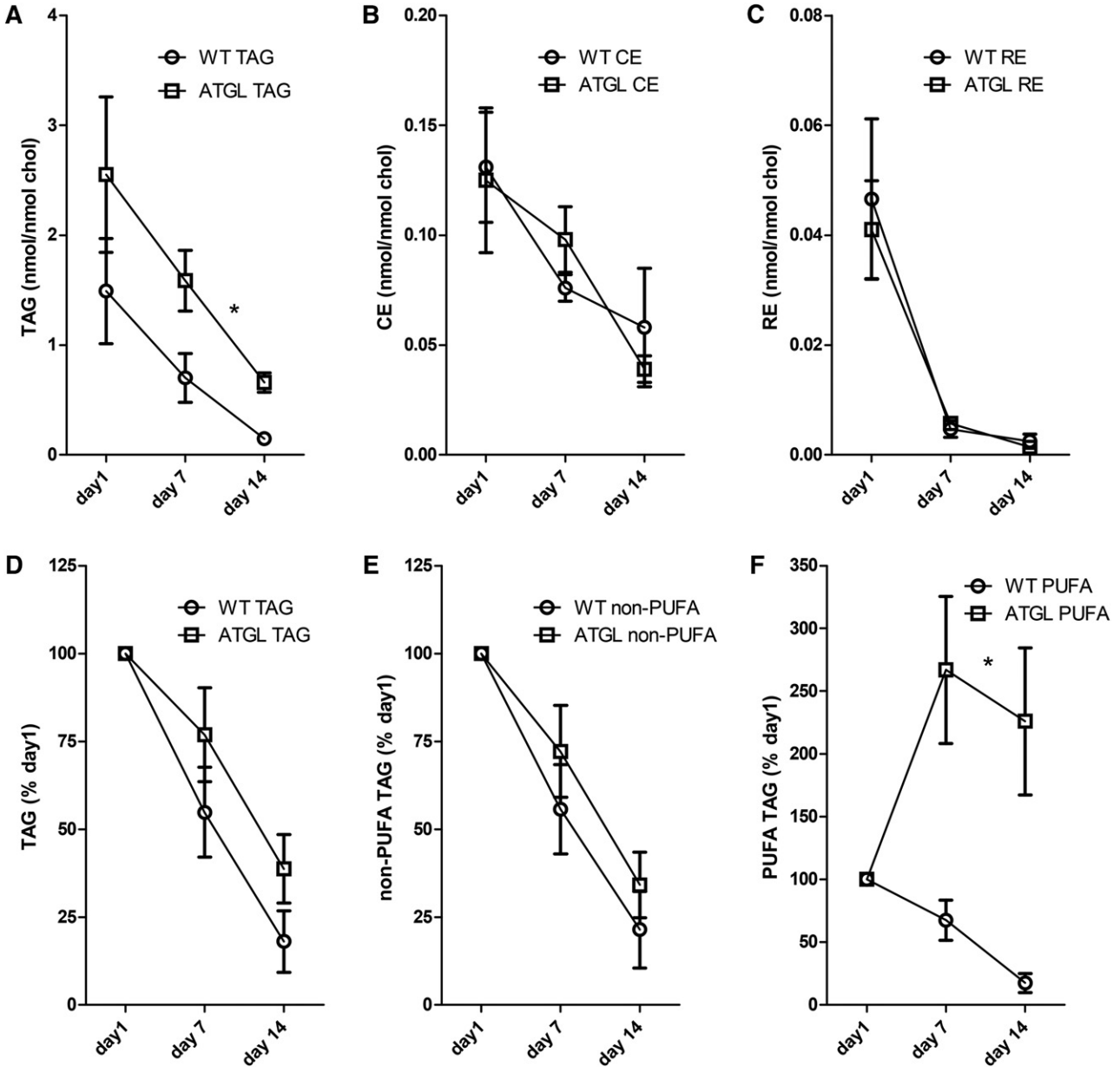

Fig. 1. Atgl deficiency has differential effect on neutral lipids in mouse HSCs. HSCs isolated from WT or *Atgl*$^{-/-}$ mice were incubated for 1, 7, or 14 days in normal medium. Subsequently, neutral lipids were determined by HPLC-MS. Values of all TAG species, TAG (A), CE (B), and RE (C), were expressed relative to the amount of cholesterol in the same sample. D–F: The relative net loss or gain of all TAG species (D), specific TAG species without a PUFA chain (E), and specific TAG species with one or more PUFA-chains (F) during the incubation as values are expressed relative to the level of the respective lipids present at day 1. Data are the mean ± SEM of six mice. *$P < 0.05$ ANOVA, WT versus *Atgl*$^{-/-}$.

predominant D4-palmitate-labeled species were the TAGs with two palmitoyl groups, from which more than 50% were labeled (Fig. 2A, first bar). ATGL is involved in the breakdown of this newly formed TAG pool, as the labeled TAG pool was lost at a significantly lower relative rate in *Atgl*$^{-/-}$ HSCs (half time >2 days) compared with WT cells (half time <1 day; Fig. 2C, gray and dark gray bars). The breakdown of nonlabeled, mainly preexisting, TAGs was not different in the ATGL-deficient cells (Fig. 2C, white bars), assuming an equal resynthesis of unlabeled TAG species during the chase in both mouse types from FAs from the medium. Similar results were observed for the predominant D8-arachidonate-labeled TAG species (Fig. 2B, C), indicating that ATGL is specific for newly formed TAGs, irrespective of the degree of unsaturation of the FA moieties.

We previously reported that the enrichment of PUFAs into newly synthesized TAGs is caused by a downregulation of the general ASCL1 isoform concomitant with an upregulation of the PUFA-specific ACSL4 isoform upon rat HSC activation (5). To see whether a similar shift occurred in mouse HSCs to explain the increase in PUFA-TAGs observed in the ATGL-deficient HSCs, we determined the relative mRNA expression of ASCL1 and ASCL4 in mouse HSCs at days 1 and 7. We found that the ratio of the ACSL4 mRNA to ASCL1 mRNA levels increased from 0.8 ± 0.2 at day 1 to 4.6 ± 0.7 at day 7 (n = 6). No difference in increase in the ASCL4/ASCL1 ratio was observed between WT and ATGL$^{-/-}$

JOURNAL OF LIPID RESEARCH

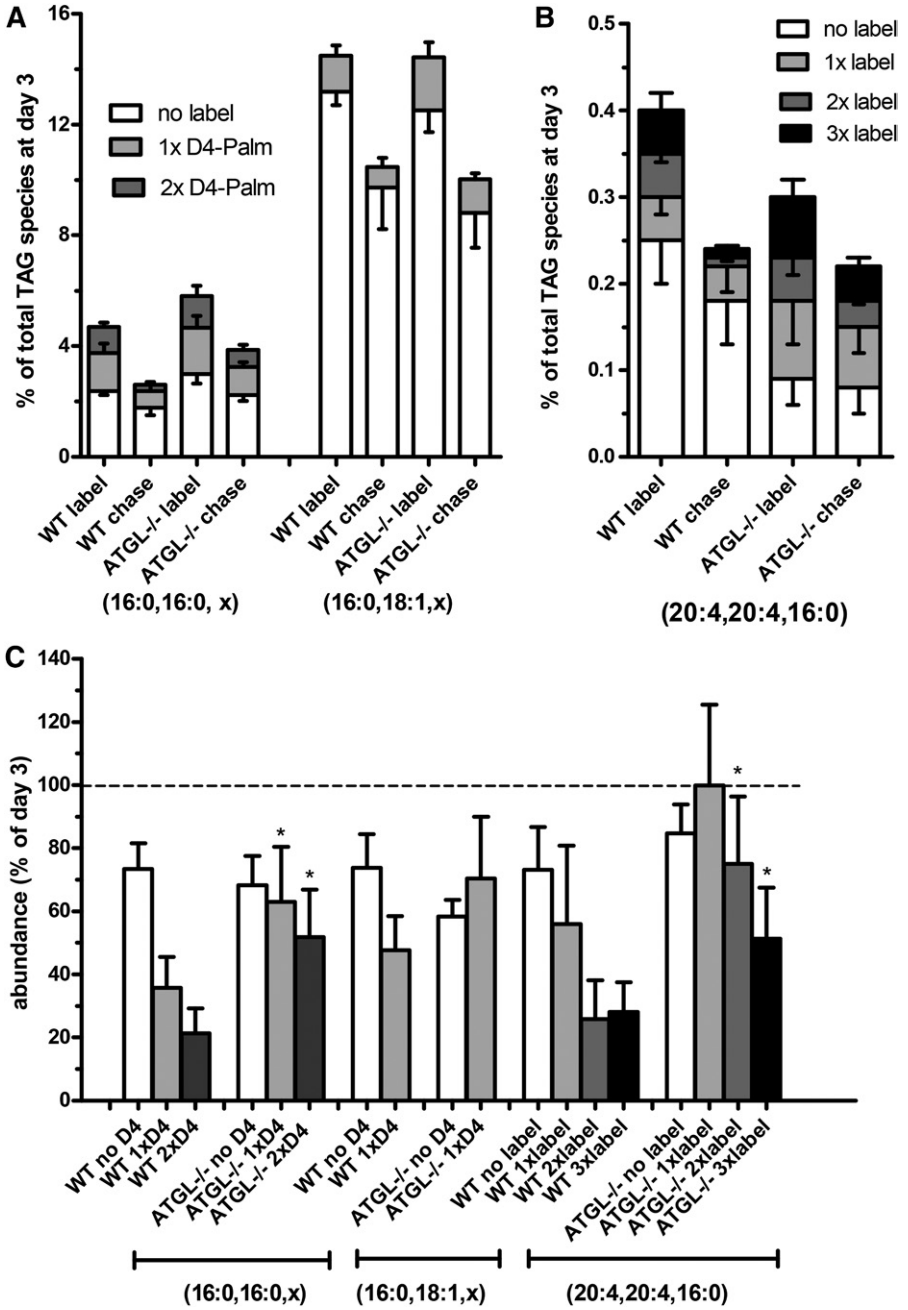

Fig. 2. Atgl-deficient mouse HSCs have a lower relative breakdown of newly labeled TAG species. A, B: Primary WT and ATGL$^{-/-}$ mouse HSCs were incubated on day 1 with D4-palmitate and D8-arachidonic acid for 2 days. At day 3, part of the cells were harvested (label) and the remaining HSCs were chased for 48 h with normal medium and harvested at day 5 (chase). Subsequently, neutral lipids were extracted and HPLC-MS was performed as described. A: Single or double deuterium-labeled (gray and dark gray bars) and nonlabeled (white bars) TAG fragments with two palmitoyl chains (16:0, 16:0, x) and a palmitoyl and an oleoyl chain (16:0, 18:1, x) were quantitated and expressed as percentage of all TAG species. B: Single, double, or triple deuterium-labeled (gray, dark gray, and black bars) and nonlabeled (white bars) forms of di-arachidonoyl-palmitoyl glycerol (20:4, 20:4, 16:0) were quantitated and expressed as percentage of all TAG species. C: Shows breakdown of the labeled TAG species as the data from the indicated TAG fragments of the cells at day 5, after the chase, were expressed relative to the level of the same TAG species at the beginning of the chase at day 3. Data are the mean ± SEM of five experiments performed in duplicate. *$P < 0.05$ *t*-test versus WT.

HSCs. This demonstrates a clear enrichment of the PUFA-specific ASCL4 isoform upon activation of mouse HSCs. Furthermore, we observed that D8-arachidonate was incorporated at a higher rate into TAG in activated HSCs at day 6 than in relatively quiescent cells at day 1 (**Fig. 3B**).

DGAT1 is involved in de novo synthesis of TAG during HSC activation

To investigate which of the two acyl-CoA:DAG acyltransferase (DGAT) enzymes was involved in the formation of the new TAG species in mouse HSCs during activation, we

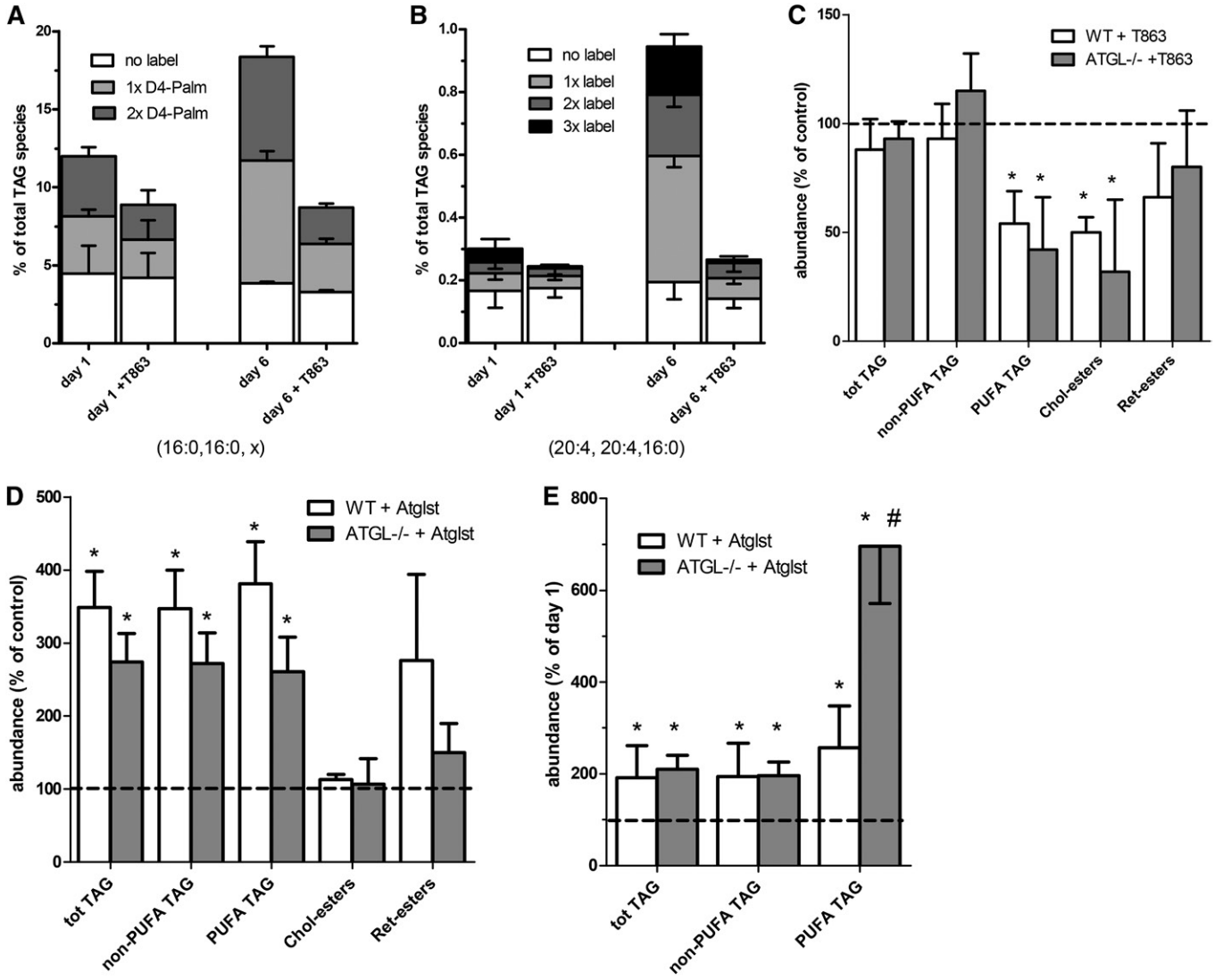

Fig. 3. Effect of the DGAT1 inhibitor, T863, and Atglistatin on TAG metabolism in WT and ATGL$^{-/-}$ mouse HSCs. A, B: HSCs isolated from WT or *Atgl*$^{-/-}$ mice were incubated on day 1 or day 6 with D4-palmitate and D8-arachidonic acid for 24 h, additionally containing vehicle (DMSO) or 20 μM T863. At day 2 or 7, the cells were harvested and neutral lipids were determined with HPLC-MS. A: Single or double deuterium-labeled (gray and dark gray bars) and nonlabeled (white bars) TAG fragments with two palmitoyl chains (16:0, 16:0, x) were quantitated and expressed as percentage of all TAG species. B: Single, double, or triple deuterium-labeled (gray, dark gray, and black bars) and nonlabeled (white bars) forms of di-arachidonoyl-palmitoyl glycerol (20:4, 20:4, 16:0) were quantitated and expressed as percentage of all TAG species. C–E: Isolated WT and ATGL-deficient mouse HSCs were incubated from day 1 to day 7 with vehicle (DMSO; control), 20 μM T863 (C), or 50 μM Atglistatin (Atglst) (D, E). The values of the various neutral lipids were normalized to the amount of cholesterol in the sample and expressed relative to the level of the respective lipids present in the control cells at day 7 (C, D), or expressed relative to the levels present at the beginning of the incubation (day 1) to show that Atglistatin causes a net increase in TAG (E). Data are the mean ± SD of three experiments performed in duplicate. C–E: *$P < 0.05$ ANOVA, treatment versus control; #$P < 0.05$ ANOVA, WT versus *Atgl*$^{-/-}$ mice.

determined the DGAT1 and DGAT2 mRNA expression in mouse HSCs at day 1 and day 7. The mRNA levels of DGAT1 were higher compared with those of DGAT2 at day 1 (relative mRNA levels of 118 ± 26 and 35 ± 36, respectively; n = 6), and the difference between DGAT1 and DGAT2 mRNA expression increased during activation at day 7 (relative mRNA levels of 136 ± 20 and 14 ± 16, respectively; n = 6). To test the role of DGAT1 on the synthesis of new TAGs, we determined the incorporation of deuterium-labeled FAs into TAG in the presence of the DGAT1-specific inhibitor, T863 (21). As shown in Fig. 3A, B, the DGAT1 inhibitor inhibited the incorporation of both D4-palmitate and D8-arachidonate into TAG. The DGAT1-specific inhibitor, T863, also caused a clear decrease in the levels of PUFA-TAGs in both WT and *Atgl*$^{-/-}$ HSCs during activation, but had almost no effect on the non-PUFA-TAG levels (Fig. 3C). This indicates that PUFAs are preferentially incorporated in the newly formed TAG pool in mice, similar to what is observed in rat HSCs. As shown in Fig. 3C, the levels of CEs were lower in T863-treated mouse HSCs, suggesting that this drug may also affect cholesterol acylation.

JOURNAL OF LIPID RESEARCH

Atglistatin inhibits the predominant lipase in mouse HSCs

The *Atgl*$^{-/-}$ mice also provided a model to study the specificity of the ATGL-specific inhibitor, Atglistatin, in HSCs (22). Surprisingly, Atglistatin treatment for 6 days resulted in an almost similar increase in TAG levels in *Atgl*$^{-/-}$ HSCs as compared with WT HSCs (Fig. 3D). This amounted to a 2-fold net increase in the total TAG levels in both WT and *Atgl*$^{-/-}$ HSCs, when compared with the original TAG levels at day 1 (Fig. 3E). This clearly demonstrates that Atglistatin not only inhibits ATGL, but also targets another, as yet unknown, TAG lipase, which plays a major role in the degradation of the TAG pool in mouse HSCs.

Effect of TAG metabolism on HSC activation

To investigate whether a change in LD size and number is causally related to the activation process, we determined the expression levels of α-SMA after the various treatments to alter TAG content of the HSCs and determined the cellular morphology of the cells. α-SMA is considered a marker for HSC activation and was clearly upregulated in mouse HSCs (**Fig. 4A**). However, neither deletion of ATGL nor addition of the lipase inhibitor, Atglistatin, or the DGAT1 inhibitor, T863, affected the expression of the activation marker, α-SMA, in mouse HSCs (Fig. 4A, B). In contrast, we observed a 30% inhibition of α-SMA expression by both Atglistatin and T863 in rat HSCs (Fig. 4B). Imaging studies show that Atglistatin increased both the number and size of LDs in rat and mouse HSCs, whereas the DGAT1 inhibitor, T863, decreased these parameters in rat HSCs (**Fig. 5**). In HSCs from WT mice, T863 had no effect on LD size or number, but T863 decreased the number of LDs in *Atgl*$^{-/-}$ HSCs (Fig. 5).

Rat HSCs have a higher TAG turnover as compared with mouse HSCs

As we observed effects of Atglistatin and the DGAT-inhibitor, T863, on activation and LD number and size in rat HSCs, we investigated neutral lipid metabolism in isolated HSCs from this rodent in more detail. The dynamics of TAG formation and degradation in rat HSCs was assessed by labeling freshly isolated rat HSCs for 2 days with deuterated FAs followed by a 1 day chase. As shown in **Fig. 6A** (sum of labeled species in first and third bar), 20% of all the TAG species were labeled with D4-palmitate after 2 days. From the TAG species containing two palmitoyl groups, even 80% was labeled (first bar). This suggests that a large part of the total TAG pool is renewed if we assume that palmitoyl-containing TAG species behave similarly to the other TAG species. Most of the label was replaced after the 24 h chase, especially in the doubly labeled TAGs, which lost more than 90% of their label (see Fig. 6A, B, chase). Similar results were observed for the D8-arachidonate-labeled TAG species upon addition of D8-arachidonate to HSCs for 2 days [results not shown; see (4)]. This indicates that rat HSCs contain a large and highly dynamic

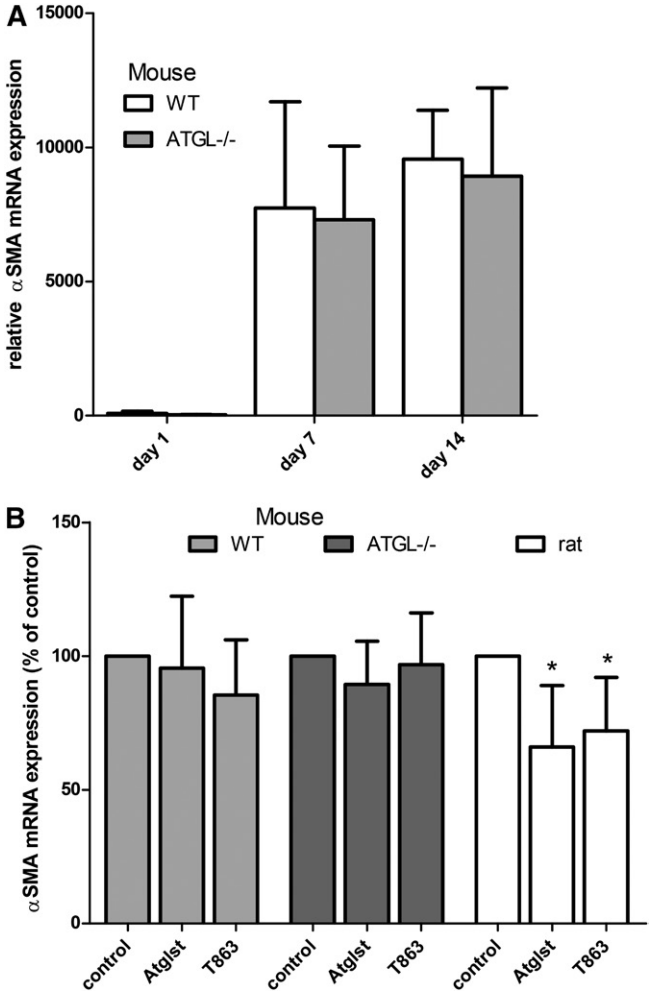

Fig. 4. Effect of alterations in TAG metabolism on activation of rat and mouse HSCs. Relative gene expression of α-SMA (HSC activation marker) was measured by qPCR. A: HSCs isolated from WT or *Atgl*$^{-/-}$ mice were incubated for 1, 7, or 14 days in normal medium (n = 6). B: HSCs isolated from WT or *Atgl*$^{-/-}$ mice or from rats were incubated from day 1 to day 7 with vehicle (DMSO; control), 50 μM Atglistatin (Atglst), or 20 μM T863. Relative mRNA levels of α-SMA were expressed relative to the levels in the control-treated cells (n = 3). Data are the mean ± SD. *$P < 0.05$ *t*-test versus control.

TAG pool with turnover rates of less than 8 h. In comparison to mouse HSCs, rat cells incorporated more labeled FAs, but also lost their newly made TAGs at a higher relative rate (compare Fig. 2A, B to Fig. 6A, B).

ATGL and DGAT1 are involved in TAG turnover in rat HSCs

Next we tested the effects of the DGAT1-specific inhibitor, T863, and Atglistatin on TAG formation and breakdown in rat HSCs. As shown in **Fig. 7A**, T863 inhibited the incorporation of D4-labeled palmitate in TAG by 80% and caused a similar decrease in the unlabeled TAGs, presumably due to inhibition of the incorporation of unlabeled palmitate from the fetal calf serum. Atglistatin prevented the breakdown of labeled TAG almost completely and also increased the level of nonlabeled TAG almost 4-fold during the 2 day chase. This latter observation was most likely

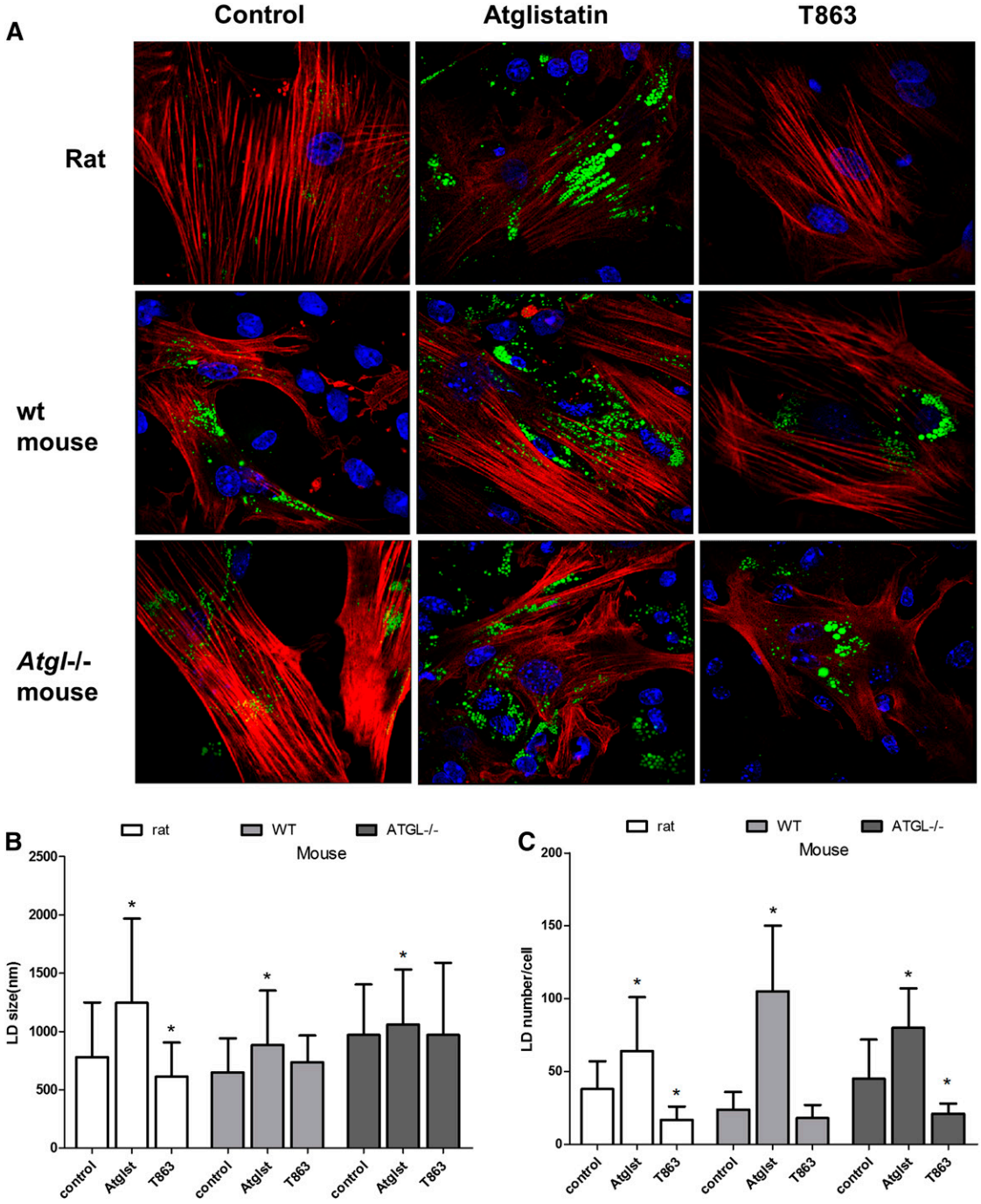

Fig. 5. Effect of Atglistatin and the DGAT1 inhibitor, T863, on LDs and on the activation marker, α-SMA, in rat and mouse HSCs. A: Confocal images of HSCs isolated from rats and WT or *Atgl*$^{-/-}$ mice, which were incubated from day 1 to day 7 with vehicle (DMSO; control), 50 μM Atglistatin (Atglst), or 20 μM T863. LDs were stained with LD540 dye (green), anti α-SMA antibody (red), and nuclei were stained with Hoechst (blue). Shown are representative pictures from three experiments. B, C: Images were analyzed with CellProfiler v2.1.1. B: LD size was expressed in diameter (nanometers). C: LD numbers were expressed as a ratio of scored LDs and scored nuclei per image. Image analysis of rat HSCs was based on 40 cells and 2,500 LDs per condition and for mouse HSCs, both WT and *Atgl*$^{-/-}$ animals, on 85 cells and 3,000 LDs per condition. Data are the mean ± SD. *$P < 0.05$ *t*-test versus control.

caused by inhibition of degradation of the newly formed unlabeled TAGs (Fig. 7A, B). When rat HSCs were incubated for 6 days with Atglistatin, the TAG levels were even 10-fold higher compared with control incubated cells (Fig. 7C). This experiment demonstrates the large capacity of rat HSCs to synthesize TAG, because net TAG formation is now unmasked by the virtual absence of the normally large concurrent degradation pathway. The DGAT1-specific inhibitor, T863, caused 80% lower TAG levels after a 6 day incubation (Fig. 7D), suggesting that DGAT1 is the principal enzyme in the high TAG formation in activated rat HSCs. The levels of CEs and REs were also lowered by T863, indicating that either these neutral lipids require the presence of the major LD core lipid, TAG, or that

JOURNAL OF LIPID RESEARCH

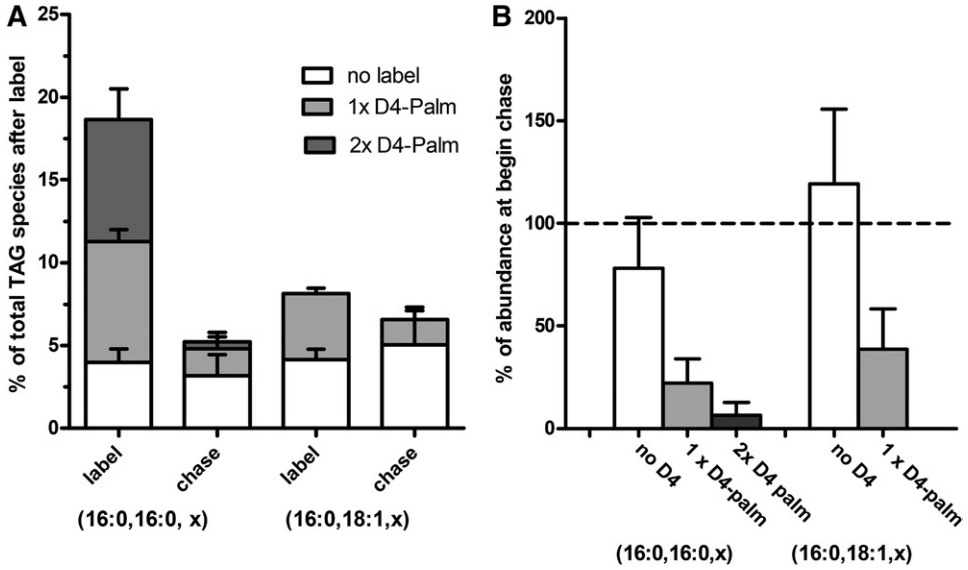

Fig. 6. High turnover of TAG in rat HSCs. A, B: Primary rat HSCs were incubated on day 1 with D4-palmitate for 2 days. At day 3, some of the cells were harvested (label) and the remaining HSCs were chased for 24 h with normal medium and harvested at day 4 (chase). Subsequently, neutral lipids were extracted and HPLC-MS was performed as described. A: Single or double deuterium-labeled (gray and dark gray bars) and nonlabeled (white bars) TAG fragments with two palmitoyl chains (16:0, 16:0, x) and a palmitoyl and an oleoyl chain (16:0, 18:1, x) were quantitated and expressed as percentage of all TAG species. B: Shows breakdown of the labeled TAG species as the data from the indicated TAG fragments of the cells at day 4, after the chase, were expressed relative to the level of the same TAG species at the beginning of the chase at day 3. Data are the mean ± SD of three experiments performed in duplicate.

T863 also affects the enzymes involved in CE and RE synthesis.

T863 and Atglistatin might be not completely specific for DGAT1 and ATGL, respectively, as was clearly found in the case of Atglistatin in mouse HSCs. Therefore, we wanted additional evidence for a role of ATGL and DGAT1 in the rapid turnover in rat HSCs. To this end, we measured the expression of various TAG-metabolizing genes in quiescent (day 1) and activated (day 7) rat HSCs. Of the tested genes, *Atgl*, in combination with its regulator, CGI-58, and *Dgat*1 are likely to play a role in the rapid rat HSC lipid turnover, as HSL mRNA was not detectable and *Dgat*2 expression was relatively low (**Fig. 8A**). We found no indication that the expression level of these genes was upregulated during activation. In contrast, ATGL expression was downregulated during the 7 day culture of the HSCs. We next explored the function of the candidate genes, *Atgl*, *Dgat*1, and *Dgat*2, by siRNA-mediated silencing. The efficiency of silencing was between 80 and 50%, as shown in Fig. 8B. In line with the mRNA expression data, knockdown of *Atgl* and *Dgat*1, but not *Dgat*2, affected the levels of TAG in rat HSCs (Fig. 8C). *Atgl* knockdown clearly inhibited the relative loss of labeled palmitate during the chase and caused a higher level of labeled palmitate-containing TAGs at the beginning of the chase, probably by an inhibition of breakdown during the labeling period (see Fig. 8D, E). A more quantitative estimation of the roles of ATGL and DGAT1 on TAG levels in rat HSCs was hampered by the relatively low knockdown efficiency in these primary cells (50% and 60%, respectively, on mRNA levels; Fig. 8B). The relatively small effects on TAG levels by the knockdown of ATGL and DGAT1 did not cause an effect on HSC activation, because we could find no effect on α-SMA expression by siRNA-mediated knockdown of *Atgl*, *Dgat*1, and *Dgat*2 in rat HSCs (Fig. 8F).

DISCUSSION

Our study with ATGL-deficient HSCs showed that ATGL has a limited, but specific, role in lipid degradation in this cell type. We could not confirm a significant role of this lipase in the degradation of REs in culture-activated mouse HSCs as suggested by Taschler et al. (23). Knockout of *Atgl* did not prevent a decrease in most TAG species without PUFA chains, but caused a preferential accumulation of PUFA-TAG species. This differential behavior was not expected, as no clear preference of ATGL for specific acyl chains has been described (24). We here propose that, rather than an acyl-chain preference, the observed difference in TAG species distribution reflects a preference of ATGL for newly synthesized TAGs, as: *i*) the degradation of newly formed TAGs was specifically decreased in the ATGL-deficient mouse HSCs; *ii*) PUFAs are preferentially incorporated in newly synthesized TAG in HSCs upon activation by an enrichment of ACSL4 (5), that we now observe also in mouse HSCsl; and *iii*) the DGAT1-specific inhibitor, T863, which inhibited the formation of new TAGs in mouse HSCs, also specifically affected the levels of PUFA-TAGs in activated mouse HSCs.

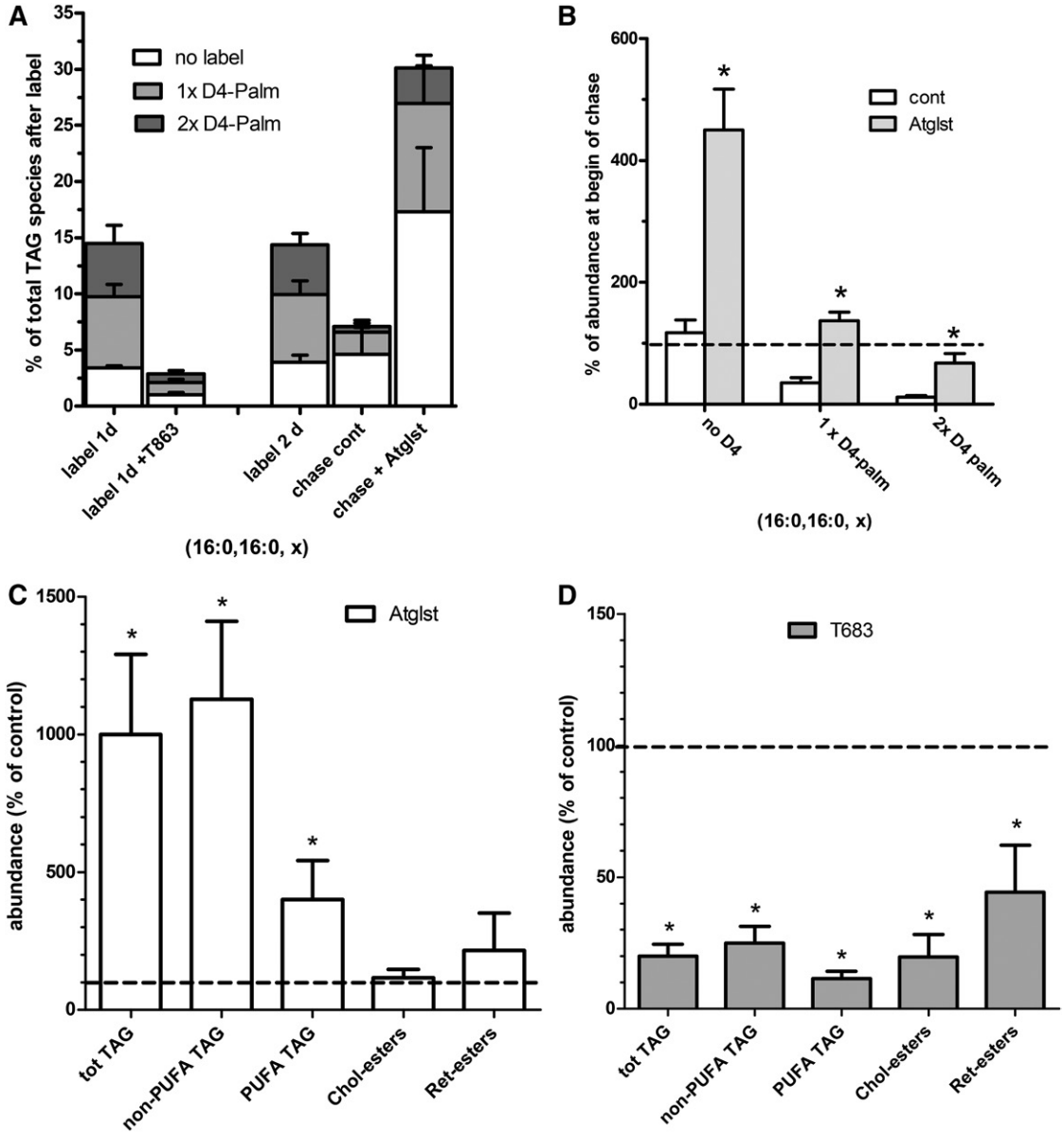

Fig. 7. Effect of Atglistatin and the DGAT1 inhibitor, T863, on TAG metabolism in rat HSCs. A, B: Isolated rat HSCs were either labeled on day 6 with D4-palmitate for 1 day in the presence or absence of 20 μM T863 (label 1d) or labeled for 2 days from day 1 to day 3 (label 2d) and subsequently chased for another 2 days in the presence of vehicle (DMSO; chase cont) or 50 μM Atglistatin (chase + Atglst). Neutral lipids were determined by HPLC-MS. A: Single or double deuterium-labeled (gray and dark gray bars) and nonlabeled (white bars) TAG fragments with two palmitoyl chains (16:0, 16:0, x) were quantitated and expressed as percentage of all TAG species. B: Shows breakdown of the D4-palmitate-labeled TAG species as the data from the cells after the chase, were expressed relative to the level of the same TAG species at the beginning of the chase. C, D: Isolated rat HSCs were incubated from day 1 to day 7 with vehicle (DMSO; control), 50 μM Atglistatin (Atglst) (C), or 20 μM T863 (D). Subsequently, neutral lipids were determined by HPLC-MS. The values were normalized to the amount of cholesterol in the sample and expressed relative to the level of the respective lipids present in the control cells at day 7. Data are the mean ± SD of three experiments performed in duplicate. $^*P < 0.05$ *t*-test versus control.

The suggestion that ATGL specifically targets newly synthesized TAGs would imply that, in activated HSCs, two pools of TAG exist: an original pool of TAG present in the relatively large preexisting LDs and a novel pool made preferential by DGAT1 in combination with ACSL4 and, thus, enriched in PUFAs. This latter pool may well be located in newly formed and, therefore, relatively small LDs. In activated rat HSCs, we previously observed that LDs reduce in size, but increase in number and are localized in cellular extensions (4). We speculated that this was caused by fission of the LDs and extensive migration to the periphery (4). Our new data favors an alternative explanation, i.e., that the apparent redistribution of LDs is due to a degradation of the lipid content (both TAGs and REs) of original LDs concurrent with a rapid resynthesis of TAGs in novel LDs by DGAT1 in the cell periphery. Interestingly, DGAT1 has been associated with the formation of small new LDs, whereas DGAT2 was involved in the enlargement of existing LDs in model cells (25).

JOURNAL OF LIPID RESEARCH

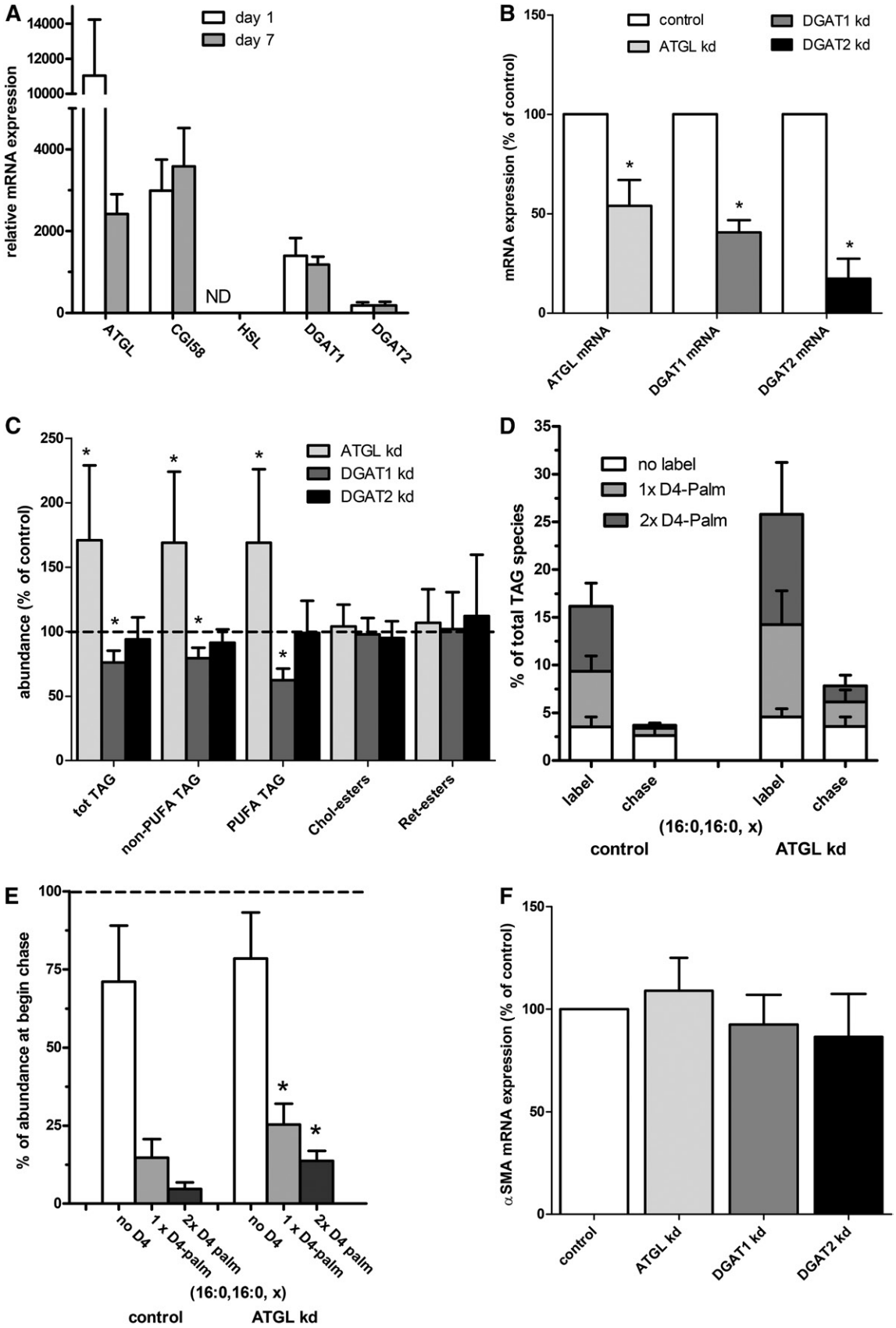

Fig. 8. *Atgl* and *Dgat*1 affects TAG metabolism in rat HSCs. A: Relative mRNA expression of genes involved in TAG breakdown and synthesis in quiescent (day 1; white bars) and activated (day 7; gray bars) rat HSCs by qPCR. B, C, F: Isolated rat HSCs were transfected at day 2 with nontargeting (control; white bars) or siRNA targeting *Atgl* (light gray bar), *Dgat*1 (gray bar), or *Dgat*2 (black bar). B: HSCs were harvested 3 days after transfection at day 5 after isolation, and relative mRNA expression of indicated genes was determined with qPCR and expressed relative to their levels in the control-transfected cells. C: Transfected HSCs were harvested on day 7 and neutral lipids were

In WT mice, the accumulation of these new PUFA-TAGs is less apparent, as this pool is probably degraded by ATGL at an equal rate as it is formed. In rat HSCs, however, the formation of new TAGs, preferentially containing PUFAs, was shown to be much higher and is apparently not balanced by ATGL. We have strong evidence that DGAT1 is a key enzyme in this rapid TAG synthesis, as TAG levels were affected by siRNA-mediated knockdown of DGAT1, but not DGAT2, in rat HSCs, and the DGAT1-specific inhibitor, T863, affected the synthesis of new TAGs and resulted in a large drop in TAG species during activation. In rat HSCs, the relatively high rate of TAG synthesis must be compensated by an almost equal rate of degradation to obtain the small net gain of TAG observed (4). The breakdown of the novel TAGs was indeed found to be very high in rat cells, as more than 80–90% of the newly formed TAGs is degraded within 1 day. Furthermore, we found that inhibition of TAG breakdown by Atglistatin caused a massive increase in total levels of TAG, which was estimated to be more than a doubling of the original amount of TAG in 1 day (as 2 days of Atglistatin resulted in a 4-fold higher level of TAG and 6 days of inhibition led to a 10-fold higher level; Fig. 7). The higher turnover of new TAGs in rat HSCs would suggest a larger role of ATGL in TAG homeostasis in rats compared with mice. This was corroborated by the clear effect of a limited siRNA-mediated knockdown of ATGL on total TAG levels (Fig. 8).

The observation that ATGL-deficient mouse HSCs still lose their TAG content indicates that another, as yet unknown, lipase is the main TAG-degrading enzyme in mouse cells. This other lipase, like ATGL, is sensitive to Atglistatin, as TAG levels were 3- to 4-fold increased by this inhibitor in both WT and *Atgl*$^{-/-}$ HSCs (Fig. 3). This would eliminate monoglyceride lipase, HSL, lipoprotein lipase, and pancreatic lipase, as well as PNPLA6 and PNPLA7, which were shown to be unaffected by this drug (22). PNPLA3, also called adiponutrin (ADPN), is also an unlikely candidate because this enzyme is involved in TAG remodeling, rather than in net lipolysis (26). In human HSCs, PNPLA3 was shown to play a role in RE degradation (27), rather than TAG breakdown. But, interestingly, a variant of this gene was associated with steatohepatitis by an as yet unknown mechanism (28). Another candidate would be lysosomal acidic lipase (LAL/Lipa), the putative TAG-degrading lipase in the lipophagy/autophagy pathway. Inhibition of autophagy was shown to result in TAG accumulation in mouse HSCs (12, 13). We have no direct information whether Atglistatin inhibits LAL/Lipa. However, we did not observe an increase in CEs after treatment with Atglistatin, as would be expected in the case of LAL/Lipa inhibition (29).

In general, this study also points out that HSCs from different species do not use metabolic pathways in a quantitatively similar way, not even in related animals such as rats and mice. This may be relevant to explain the differences observed between mice and rats in the effect of strategies to alter lipid metabolism on HSC activation. The detection of two potent inhibitors of TAG synthesis and degradation in rat HSCs, T863 and Atglistatin, respectively, allowed us to address the question of whether a change in TAG metabolism is causally related to the activation process in rat and mouse HSCs. Intriguingly, both inhibitors significantly attenuated activation in rat HSCs to a similar, albeit relatively low degree (30%, Fig. 4). Although we cannot exclude the possibility that these drugs affect HSC activation by other non-lipid-related pathways, their effects on HSC activation correlated with their effect on TAG levels, as Atglistatin and T863 had less effect on TAG levels in mouse HSCs and did not affect the expression of the activation marker, α-SMA, in these cells. As inhibition of TAG formation had the same effect as inhibiting its breakdown, rat HSCs seem to require an available TAG pool for optimal functioning. This pool may act as a buffer for FAs required for energy (13), or synthesis of membranes or bioactive lipids, like prostanoids (5). Our study with the DGAT-specific inhibitor, T863, is in line with previous studies showing that knockdown of *Dgat*1 in rat liver inhibited activation of HSCs in vitro (30), whereas knockout of *Dgat*1 in mice had no effect on subsequent HSC activation in culture (31). Interestingly, the latter study also indicated that a limited effect in vitro might be meaningful in vivo, as the DGAT1-deficient mice were less sensitive to induction of liver fibrosis (31).

The authors would like to acknowledge Jeroen Jansen for technical assistance with the lipid analysis and R. Zechner (University of Graz, Austria) for the kind donation of the *Atgl*$^{+/-}$ mice. Real-time qPCR was performed and mouse reference gene primers were provided by the Department of Clinical Sciences of Companion Animals, Faculty of Veterinary Medicine, Utrecht University. Images were acquired at the Center of Cellular Imaging, Faculty of Veterinary Medicine, Utrecht University on a Leica TCS SPE-II confocal microscope and we thank Esther van't Veld for assistance.

determined by HPLC-MS. The values were normalized to the amount of cholesterol in the sample and expressed relative to the level of the respective lipids present in the control-transfected cells. D, E: Isolated HSCs were transfected at day 2 with nontargeting (control) or siRNA targeting ATGL. One day after transfection, cells were incubated with D4-palmitate for 2 days from day 3 to day 5. After the labeling period, some of the cells were harvested (label) and the remaining HSCs were chased for 2 days with normal medium from day 5 to day 7 (chase). Subsequently, neutral lipids were determined by HPLC-MS. D: Single or double deuterium-labeled (gray and dark gray bars) and nonlabeled (white bars) TAG fragments with two palmitoyl chains (16:0, 16:0, x) were quantitated and expressed as percentage of all TAG species. E: Shows breakdown of the D4-palmitate-labeled TAG species as the data from the cells after the chase, were expressed relative to the level of the same TAG species at the beginning of the chase. F: Transfected HSCs were harvested on day 7 and relative mRNA levels of α-SMA were measured by qPCR and were expressed relative to the levels in the control-transfected cells. All data are the mean ± SD of three experiments performed in duplicate. *$P < 0.05$ *t*-test versus control.

REFERENCES

1. Blaner, W. S., S. M. O'Byrne, N. Wongsiriroj, J. Kluwe, D. M. D'Ambrosio, H. Jiang, R. F. Schwabe, E. M. Hillman, R. Piantedosi, and J. Libien. 2009. Hepatic stellate cell lipid droplets: a specialized lipid droplet for retinoid storage. *Biochim. Biophys. Acta.* **1791:** 467–473.
2. Friedman, S. L. 2008. Hepatic stellate cells: protean, multifunctional, and enigmatic cells of the liver. *Physiol. Rev.* **88:** 125–172.
3. Pellicoro, A., P. Ramachandran, J. P. Iredale, and J. A. Fallowfield. 2014. Liver fibrosis and repair: immune regulation of wound healing in a solid organ. *Nat. Rev. Immunol.* **14:** 181–194.
4. Testerink, N., M. Ajat, M. Houweling, J. F. Brouwers, V. V. Pully, H. J. van Manen, C. Otto, J. B. Helms, and A. B. Vaandrager. 2012. Replacement of retinyl esters by polyunsaturated triacylglycerol species in lipid droplets of hepatic stellate cells during activation. *PLoS One.* **7:** e34945.
5. Tuohetahuntila, M., B. Spee, H. S. Kruitwagen, R. Wubbolts, J. F. Brouwers, C. H. van de Lest, M. R. Molenaar, M. Houweling, J. B. Helms, and A. B. Vaandrager. 2015. Role of long-chain acyl-CoA synthetase 4 in formation of polyunsaturated lipid species in hepatic stellate cells. *Biochim. Biophys. Acta.* **1851:** 220–230.
6. Wilfling, F., J. T. Haas, T. C. Walther, and R. V. Farese, Jr. 2014. Lipid droplet biogenesis. *Curr. Opin. Cell Biol.* **29:** 39–45.
7. Long, A. P., A. K. Manneschmidt, B. VerBrugge, M. R. Dortch, S. C. Minkin, K. E. Prater, J. P. Biggerstaff, J. R. Dunlap, and P. Dalhaimer. 2012. Lipid droplet de novo formation and fission are linked to the cell cycle in fission yeast. *Traffic.* **13:** 705–714.
8. Zechner, R., P. C. Kienesberger, G. Haemmerle, R. Zimmermann, and A. Lass. 2009. Adipose triglyceride lipase and the lipolytic catabolism of cellular fat stores. *J. Lipid Res.* **50:** 3–21.
9. Schweiger, M., A. Lass, R. Zimmermann, T. O. Eichmann, and R. Zechner. 2009. Neutral lipid storage disease: genetic disorders caused by mutations in adipose triglyceride lipase/PNPLA2 or CGI-58/ABHD5. *Am. J. Physiol. Endocrinol. Metab.* **297:** E289–E296.
10. Eichmann, T. O., L. Grumet, U. Taschler, J. Hartler, C. Heier, A. Woblistin, L. Pajed, M. Kollroser, G. Rechberger, G. G. Thallinger, et al. 2015. ATGL and CGI-58 are lipid droplet proteins of the hepatic stellate cell line HSC-T6. *J. Lipid Res.* **56:** 1972–1984.
11. Mello, T., A. Nakatsuka, S. Fears, W. Davis, H. Tsukamoto, W. F. Bosron, and S. P. Sanghani. 2008. Expression of carboxylesterase and lipase genes in rat liver cell-types. *Biochem. Biophys. Res. Commun.* **374:** 460–464.
12. Thoen, L. F., E. L. Guimaraes, L. Dolle, I. Mannaerts, M. Najimi, E. Sokal, and L. A. van Grunsven. 2011. A role for autophagy during hepatic stellate cell activation. *J. Hepatol.* **55:** 1353–1360.
13. Hernández-Gea, V., Z. Ghiassi-Nejad, R. Rozenfeld, R. Gordon, M. I. Fiel, Z. Yue, M. J. Czaja, and S. L. Friedman. 2012. Autophagy releases lipid that promotes fibrogenesis by activated hepatic stellate cells in mice and in human tissues. *Gastroenterology.* **142:** 938–946.
14. Kluwe, J., N. Wongsiriroj, J. S. Troeger, G. Y. Gwak, D. H. Dapito, J. P. Pradere, H. Jiang, M. Siddiqi, R. Piantedosi, S. M. O'Byrne, et al. 2011. Absence of hepatic stellate cell retinoid lipid droplets does not enhance hepatic fibrosis but decreases hepatic carcinogenesis. *Gut.* **60:** 1260–1268.
15. Haemmerle, G., A. Lass, R. Zimmermann, G. Gorkiewicz, C. Meyer, J. Rozman, G. Heldmaier, R. Maier, C. Theussl, S. Eder, et al. 2006. Defective lipolysis and altered energy metabolism in mice lacking adipose triglyceride lipase. *Science.* **312:** 734–737.
16. Riccalton-Banks, L., R. Bhandari, J. Fry, and K. M. Shakesheff. 2003. A simple method for the simultaneous isolation of stellate cells and hepatocytes from rat liver tissue. *Mol. Cell. Biochem.* **248:** 97–102.
17. van Steenbeek, F. G., L. Van den Bossche, G. C. Grinwis, A. Kummeling, I. H. van Gils, M. J. Koerkamp, D. van Leenen, F. C. Holstege, L. C. Penning, J. Rothuizen, et al. 2013. Aberrant gene expression in dogs with portosystemic shunts. *PLoS One.* **8:** e57662.
18. Aardema, H., F. Lolicato, C. H. van de Lest, J. F. Brouwers, A. B. Vaandrager, H. T. van Tol, B. A. Roelen, P. L. Vos, J. B. Helms, and B. M. Gadella. 2013. Bovine cumulus cells protect maturing oocytes from increased fatty acid levels by massive intracellular lipid storage. *Biol. Reprod.* **88:** 164.
19. Bligh, E. G., and W. J. Dyer. 1959. A rapid method of total lipid extraction and purification. *Can. J. Biochem. Physiol.* **37:** 911–917.
20. Retra, K., O. B. Bleijerveld, R. A. van Gestel, A. G. Tielens, J. J. van Hellemond, and J. F. Brouwers. 2008. A simple and universal method for the separation and identification of phospholipid molecular species. *Rapid Commun. Mass Spectrom.* **22:** 1853–1862.
21. Cao, J., Y. Zhou, H. Peng, X. Huang, S. Stahler, V. Suri, A. Qadri, T. Gareski, J. Jones, S. Hahm, et al. 2011. Targeting acyl-CoA:diacylglycerol acyltransferase 1 (DGAT1) with small molecule inhibitors for the treatment of metabolic diseases. *J. Biol. Chem.* **286:** 41838–41851.
22. Mayer, N., M. Schweiger, M. Romauch, G. F. Grabner, T. O. Eichmann, E. Fuchs, J. Ivkovic, C. Heier, I. Mrak, A. Lass, et al. 2013. Development of small-molecule inhibitors targeting adipose triglyceride lipase. *Nat. Chem. Biol.* **9:** 785–787.
23. Taschler, U., R. Schreiber, C. Chitraju, G. F. Grabner, M. Romauch, H. Wolinski, G. Haemmerle, R. Breinbauer, R. Zechner, A. Lass, et al. 2015. Adipose triglyceride lipase is involved in the mobilization of triglyceride and retinoid stores of hepatic stellate cells. *Biochim. Biophys. Acta.* **1851:** 937–945.
24. Eichmann, T. O., M. Kumari, J. T. Haas, R. V. Farese, Jr., R. Zimmermann, A. Lass, and R. Zechner. 2012. Studies on the substrate and stereo/regioselectivity of adipose triglyceride lipase, hormone-sensitive lipase, and diacylglycerol-O-acyltransferases. *J. Biol. Chem.* **287:** 41446–41457.
25. Wilfling, F., H. Wang, J. T. Haas, N. Krahmer, T. J. Gould, A. Uchida, J. X. Cheng, M. Graham, R. Christiano, F. Frohlich, et al. 2013. Triacylglycerol synthesis enzymes mediate lipid droplet growth by relocalizing from the ER to lipid droplets. *Dev. Cell.* **24:** 384–399.
26. Ruhanen, H., J. Perttila, M. Holtta-Vuori, Y. Zhou, H. Yki-Jarvinen, E. Ikonen, R. Kakela, and V. M. Olkkonen. 2014. PNPLA3 mediates hepatocyte triacylglycerol remodeling. *J. Lipid Res.* **55:** 739–746.
27. Pirazzi, C., L. Valenti, B. M. Motta, P. Pingitore, K. Hedfalk, R. M. Mancina, M. A. Burza, C. Indiveri, Y. Ferro, T. Montalcini, et al. 2014. PNPLA3 has retinyl-palmitate lipase activity in human hepatic stellate cells. *Hum. Mol. Genet.* **23:** 4077–4085.
28. Krawczyk, M., P. Portincasa, and F. Lammert. 2013. PNPLA3-associated steatohepatitis: toward a gene-based classification of fatty liver disease. *Semin. Liver Dis.* **33:** 369–379.
29. Du, H., M. Duanmu, D. Witte, and G. A. Grabowski. 1998. Targeted disruption of the mouse lysosomal acid lipase gene: long-term survival with massive cholesteryl ester and triglyceride storage. *Hum. Mol. Genet.* **7:** 1347–1354.
30. Yamaguchi, K., L. Yang, S. McCall, J. Huang, X. X. Yu, S. K. Pandey, S. Bhanot, B. P. Monia, Y. X. Li, and A. M. Diehl. 2008. Diacylglycerol acyltranferase 1 anti-sense oligonucleotides reduce hepatic fibrosis in mice with nonalcoholic steatohepatitis. *Hepatology.* **47:** 625–635.
31. Yuen, J. J., S. A. Lee, H. Jiang, P. J. Brun, and W. S. Blaner. 2015. DGAT1-deficiency affects the cellular distribution of hepatic retinoid and attenuates the progression of CCl4-induced liver fibrosis. *Hepatobiliary Surg. Nutr.* **4:** 184–196.